Master's Thesis

Observation of lyotropic chromonic liquid crystals droplets with the perpendicular boundary condition

Leekyo Jung

Department of Physics

Graduate School of UNIST

2019

Observation of lyotropic chromonic liquid crystals droplets with the perpendicular boundary condition

Leekyo Jung

Department of Physics

Graduate School of UNIST

Observation of lyotropic chromonic liquid crystals droplets with the perpendicular boundary condition

A thesis/dissertation
submitted to the Graduate School of UNIST
in partial fulfillment of the
requirements for the degree of
Master of Science

Leekyo Jung

December 6, 2018 of submission
Approved by

_____

Advisor
Joonwoo Jeong

Observation of lyotropic chromonic liquid crystals droplets with the perpendicular boundary condition

Leekyo Jung

This certifies that the thesis/dissertation of Leekyo Jung is approved.

December 6, 2018 of submission

Signature

_____

Advisor: Joonwoo Jeong

Signature

_____

Hyuk Kyu Pak

Signature

_____

Chung Hun Park

Abstract

Controlling anchoring conditions of liquid crystals (LCs) is crucial for the study of liquid crystals and development of liquid crystals-based displays and sensors. Although many studies have been made on thermotropic liquid crystals, the anchoring conditions of lyotropic chromonic liquid crystals (LCLCs) are difficult to control even through properties of LCLCs were actively studied. Conventional alignment methods have no effect on LCLCs, even work, anchoring is very weak. Only a few perpendicular alignment layers (a.k.a. homeotropic anchoring) in solid-LCs interfaces were reported through non-covalent interactions of hydrophobic polymer films and solid substrates such as graphene. However, the vertical alignment layers of LCLCs at the liquid interface has never been reported.

We report, for the first time, the study of the homeotropic anchoring of liquid and LCLCs interfaces using hydrophobic oils without surfactants. As reported in thermotropic liquid crystals, a radial structure with a point defect has been found, but an unusual feature is the axial structure with ring disclination, which did not apply the external field. It implies that this anchoring strength is very weak anchoring conditions and another supporting evidence is the anchoring transition, which changes to the horizontal orientation from the perpendicular orientation. Also, because of the weak twist modulus of the LCLCs, the structure of the defects seemed to be twisted. This twist structure is consistent with previous reports. To observe the structures of homeotropic chiral nematic, brucine sulfate was used as a chiral dopants. Basically, we reproduced the director configurations of the droplets of the thermotropic chiral nematic LCs both with planar and homeotropic anchoring. Specifically, with the homeotropic anchoring, we noticed an increase in the effective helical pitch in the droplets according to the droplet size, i.e. the untwisting of the helical structure, which originates from the frustration of chiral nematic liquid crystals with the perpendicular boundary condition.

Contents

List of Figures

List of Tables

Predicates and abbreviations

BHM	Brucine Hydrochloride Monohydrate
BSH	Brucine Sulfate Heptahydrate
CLCs	Chiral (nematic) Liquid Crystals
cSt	Centistokes
HTP	Helical twisting power
LCs	Liquid Crystals
LCLCs	Lyotropic Chromonic Liquid Crystals
POM	Polarized optical microscopy
Si oil	Silicone oil
SSY (or SY)	Sunset yellow
TLCs	Thermotropic Liquid Crystals

I. Introduction

The liquid crystals are literally anisotropic liquids that have both properties between liquid and solid crystal. The Structures of LCs are determined by temperature, concentration (in case of LCLCs), external field, anchoring of LCs, and geometry of confined interfaces. Since it is possible to interact with various factors, the studies and applications have been carried out utilizing the optical / electromagnetic/ topological / fluidic properties of LCs. For example, it has been applied in various ranges such as the display panels (LCD) [1], [2], micro-laser [3] using the optical and electromagnetic properties of LCs, the biosensor [4], [5] using the phase transition of LCs. In addition, the study on liquid crystals has been focused on topology such as the chiral symmetry breaking and topological defects.

The Phase of thermotropic LCs determines by only temperature however the phase of lyotropic chromonic liquid crystals (LCLCs) is determined not only by temperature but also by concentration. It is usually used to dissolve the proper concentration in water. The ionized molecules are pi-pi stacked by non-covalent bonding to aggregates and define them as directors. [6] The physical properties of LCLCs are quite different compared to TLCs. The equilibrium structure in a nematic liquid crystal is described by the elastic free energy, which is composed of the term for each deformation mode -; splay K_1, twist K_2, bend K_3 ,and saddle-splay K_{24}. The LCLCs has a small twist modulus, a very large saddle-splay modulus, and a unique structure.

II. Theoretical background

2.1 Liquid Crystals (LCs)

2.1.1 Classification of LCs phases

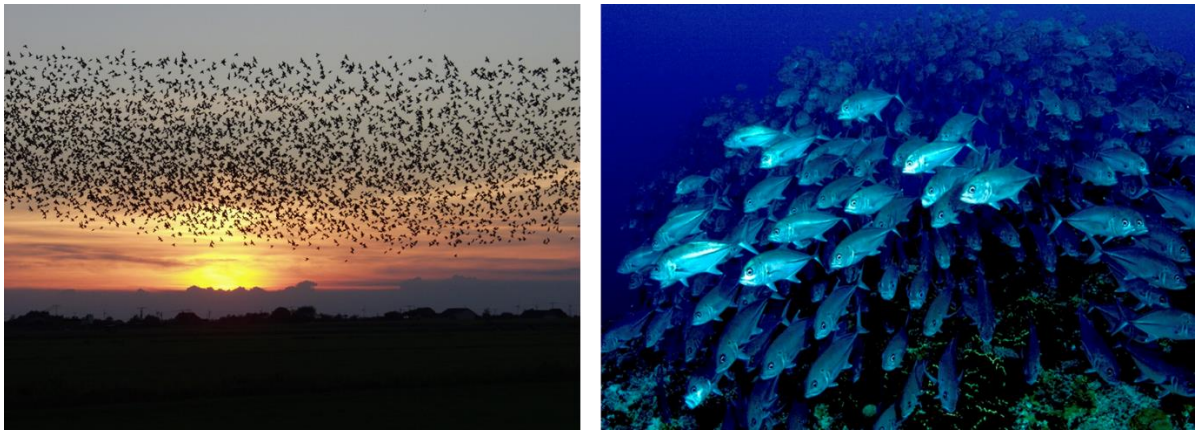

Figure 1 (left) Flock of bird [7] , (right) Shoaling of fish [8]

Liquid crystals are phases under flow like conventional liquids, but also have orientational and some of positional order. For example to metaphor, considering a group of wild animals changes their arrangements along the flowing winds or water streams to minimize a friction and their energy. In addition, if external factors change due to sudden changes in flow, attack by other predators, and changes in temperature, etc. they change a crowd to minimizes external threat. Similarly, a liquid crystal is an anisotropic liquid with collective motion, and the shape of the liquid crystal molecules is arranged like a rod or disk. [9] As in Fig. 2, the phase of the liquid crystal is determined by the temperature and concentration (in the case of lyotropic LCs). It is also possible to have various interactions with optical [10], electromagnetic [11], topological [12], and fluid properties [13].

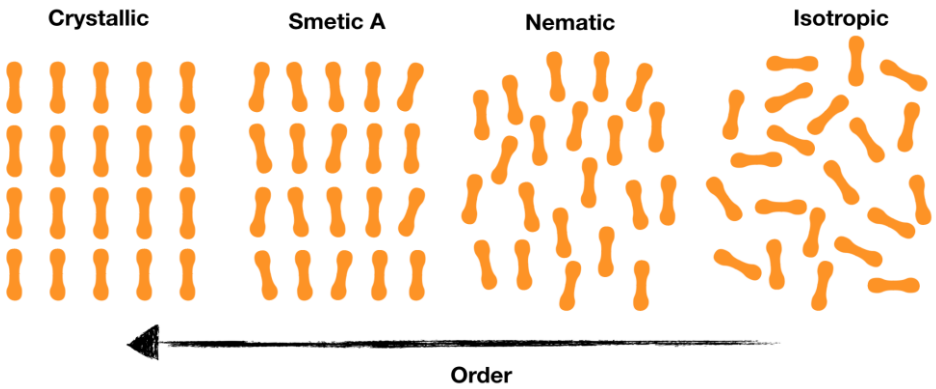

Figure 2 Phase schematics of rod like liquid crystals.

2.1.2 Order of nematic LCs

Conventionally, the way to express the order of liquid crystals describes the orientation of the liquid crystal molecules as an average. [14] Traceless, symmetric tenser Q

$$\mathbf{Q_{ij}} = \frac{S}{2}(\mathbf{3n_i n_j - \delta_{ij}}) \quad (1)$$

Where the scalar order parameter S,

$$\mathbf{S} = \frac{1}{2} < \mathbf{3\cos^2\theta - 1} > \quad (2)$$

is expressed in terms of Legendre polynomial P_2 , and is described by the degree of ordering of the system. Where θ represents the average direction and the angle of the liquid crystal molecules, and S is the largest eigenvalue of Q. Also, the eigenvector n of Q is called director. Director is a unit vector and has headless property **n** = -**n**. [15]

2.1.3 Elastic free energy

The Structures of confined liquid crystals has a structure that minimizes the total free energy.

$$\mathbf{F} = \int \left(\boldsymbol{f_{homogeneous} + f_{elastic} + f_{rapini}}\right)\boldsymbol{dV} \quad (3)$$

where each free energy density, $f_{homogeneous}$ represents the internal energy of nematic liquid crystals without the distortion, $f_{elastic}$ described in term related to elastic deformation, and last term, f_{rapini} implies the interaction of the liquid crystals and interface. [16] Here we have to focus at last two term.

Frank-Oseen elastic free energy [14], [15], [17]

$$f_{elastic} = \frac{1}{2}[\ \mathrm{K_1}\ (\nabla \cdot \mathbf{n})^2 + \ \mathrm{K_2}\ (\mathbf{n} \cdot \nabla \times \ \mathbf{n})^2 + \mathrm{K_3}\ (\mathbf{n} \times \nabla \times \ \mathbf{n})^2 - \mathrm{K_{24}}\ \nabla \cdot (\mathbf{n}(\nabla \cdot \mathbf{n}) + \mathbf{n} \times \nabla \times \ \mathbf{n})] \quad (4)$$

is consisted of 4 elastic constant. it is related in each elastic deformation mode – Splay , twist ,and bend on Fig.3 [18]. The configuration of liquid crystals is minimized to elastic free energy for each deformations. Indeed, because the elastic constants are intrinsic properties depending on liquid crystals or phase (temperature , concentration, additives, etc.), This suggests that the preferred deformation for the elastic constants.

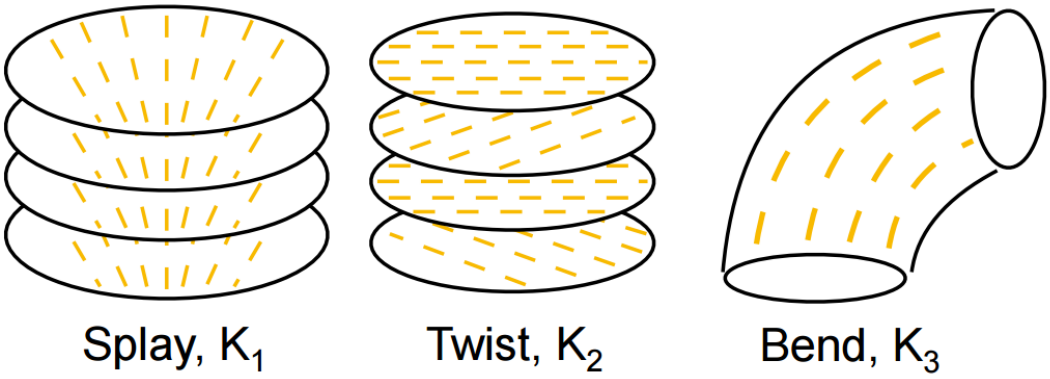

Figure 3 The elastic deformation of liquid crystals

Last term, the rapini model is discussed in detail in Section 2.3.2.

2.2 Chiral Nematic Liquid Crystals

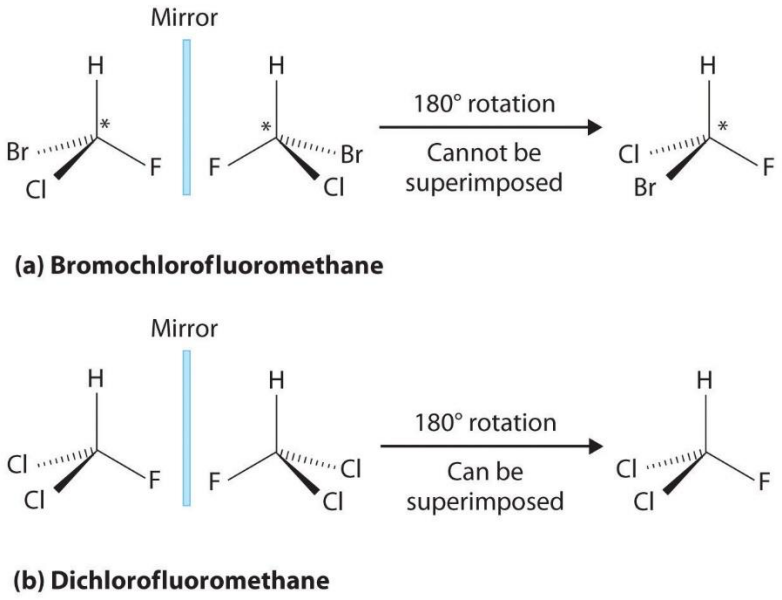

Figure 4 Comparison of Chiral and Achiral molecules. (a) Bromochlorofluoromethane is chiral and (b) Dichlorofluoromethane is achiral. [19]

The original meaning of Chirality was obtained in Greek "χεῖρ" (kheir) meaning hand. [20] Chirality in physical concepts refers to 'non-superimposable molecules', suggesting that the mirror image (other called enantiomers or optical isomers) is not the same as the original molecule.[19] Chiral (or cholesteric) nematic phase N * is closely connected with the nematic phase. However, unlike nematic, chiral nematic has the property that the director is twisted about perpendicular molecular axis. (see Fig.5)

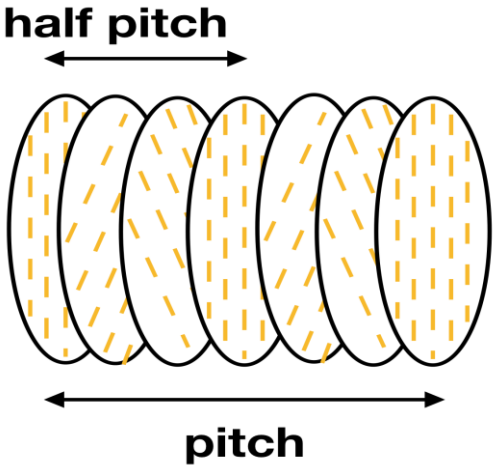

Figure 5 Schematics of the chiral nematic phase layer. Yellow rod represents the director of liquid crystals. The chiral pitch is a distance which the director rotate 2π turn.

The chiral pitch (shortly, pitch) is defined as the distance that liquid crystal molecules experienced 2 π turn. In the chiral nematic phase, the twist energy term of Elastic free energy is modified. Rewriting the chiral nematic f_2,

$$\boldsymbol{f_2 = \frac{K_2}{2}\left[\left(\mathbf{n}\cdot\nabla\times\mathbf{n}+\frac{2\pi}{p_0}\right)\right]^2 = \frac{K_2}{2}\left[(\mathbf{n}\cdot\nabla\times\mathbf{n}+q_0)\right]^2} \quad (5)$$

where inverse cholesteric pitch q_0 represents a wave vector in the chiral nematic phase layer, as in optics. The director configuration of the ground state is twisted by pitch to offset the added q0. If q_0 is positive sign, it means right-handiness rotation, and when it is negative sign, it means left -handiness rotation. The chiral pitch can also be changed depending on the condition(temperature, geometry).

$$\mathbf{p_0} = \frac{1}{c\cdot HTP} \quad (6)$$

where c is the concentration of the chiral dopants (wt /wt), HTP is the helical twisting power, and HTP is depending on the liquid crystal and dopants. It also mainly depends on the temperature.[9] As mentioned above, it can be seen similar to optics, but pitch is replaced with wavelength. For this reason, chiral nematic liquid crystals are widely used in optical applications such as Bragg reflection and blue phases. [20]–[22]

2.3 Lyotropic Chromonic Liquid Crystals (LCLCs)

2.3.1 Properties of LCLCs

Lyotropic chromonic liquid crystals (LCLCs) are dependent on both temperature and concentration phase, unlike Thermotropic LCs (TLCs), in which phase only temperature is determined. In some examples of LCLCs, there are Sunset yellow, DSCG, Allura red, Acid yellow 23, Blue 27, Violet 20. The LCLCs molecules are amphiphilic, for example, Sunset yellow (SSY) has hydrophilic (water - soluble) at the edges, hydrophobic core. Notice the implication of the name of LCLCs. The word 'lyo-' means 'dissolve' in Greek, and as in Fig.6, molecules are ionized into self-assembly (chromonic) and form a liquid crystal phase.

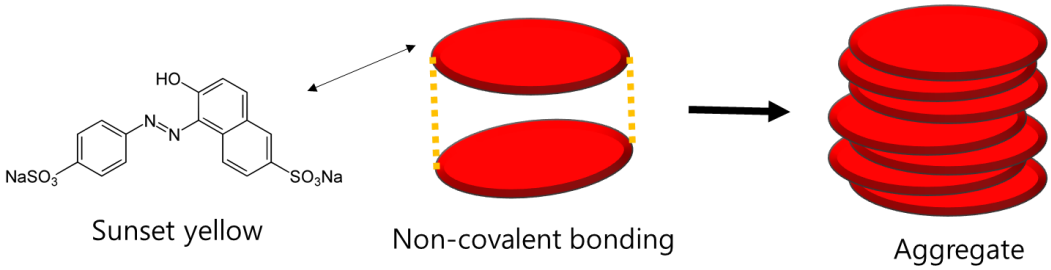

Figure 6 Sunset yellow and schematics of ionized (dissolved to water) sunset yellow

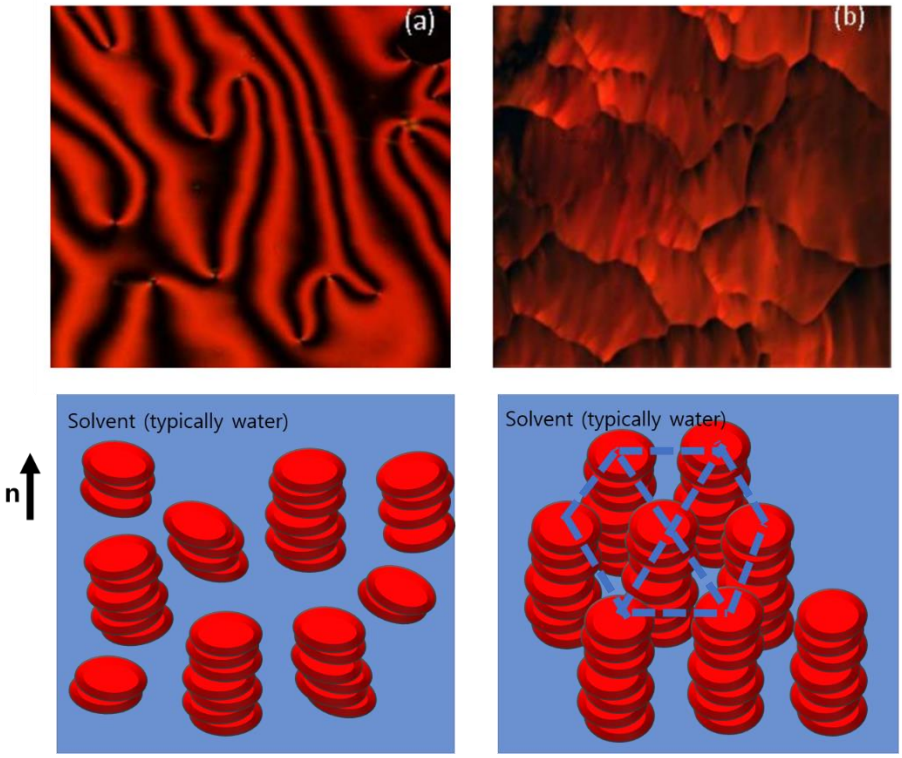

Figure 7 (a) Nematic (30% [wt/wt]) and (b) Columnar phase (40% [wt/wt]) of SSY. Bottom schematics shows the order of each phases. [23]

K(pN) At 25℃	**Splay K_1**	**Twist K_2**	**Bend K_3**	**Saddle-splay K_{24}**
5CB	6.6	3.0	10	~10
Sunset Yellow (SSY, 31.5wt%)	8.4	**0.8**	8.1	**~50**
Disodium Cromoglycate (DSCG, 14wt%)	8	**0.6**	18	**13.5 ~ 31.5**

Table 1 Elastic modulus of 5CB , SSY, DSCG [24]–[27]

In case of the thermotropic LCs, the director defined as a local average direction of LC molecules. However , the director of LCLCs is a local average direction of aggregates. The diameter of SSY aggregates is about 1-2nm and distance between molecules in aggregates is 0.34nm. [28]
The length of aggregates $L \propto \exp\left(\frac{E}{2k_BT}\right)$ [29], it is inverse proportion to the temperature and proportional to the concentration c. As shown in Fig. 7, the order of LCLCs become larger as longer the length of Aggregates. See Fig. 7.b, in the columnar phase, the twist deformation is limited ($K_2 \rightarrow \infty$), resulting in a roughly hexagonal lattice structure. [30] Interestingly, referring to Table 1, the elastic constant of LCLCs (SSY,DSCG) has a small twist modulus and a very large saddle-splay modulus compared to the thermotropic LCs (5CB). Thus, LCLCs can have a unique director structure.

2.3.2 Anchoring of LCLCs

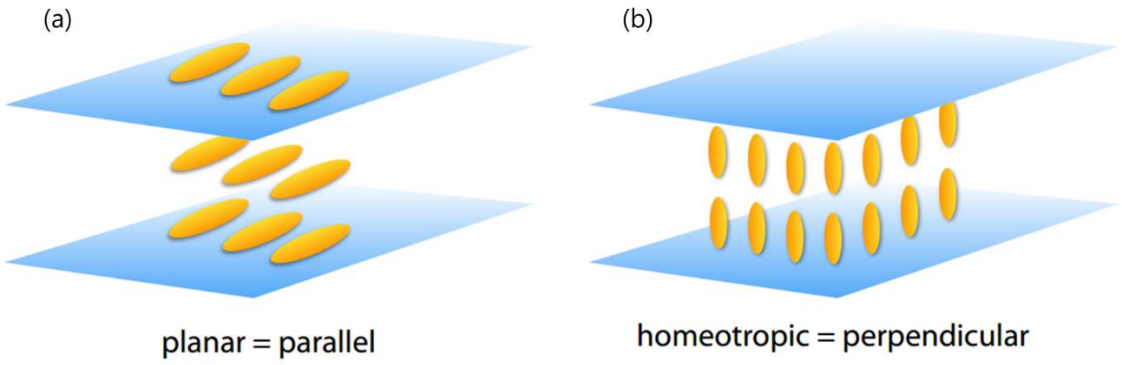

Figure 8 Examples of anchoring condition. (a) planar anchoring is parallel to the surface (b) homeotropic anchoring is perpendicular to the surface.

The most important factor for studying liquid crystals and developing applications is controlling anchoring. The elastic interaction at the boundary condition of the liquid crystal is propagated to the bulk and the structure of the director is formed. The parallel orientation is called planar anchoring and is called degenerate planar if there is no preferred direction. (Fig.8.a). The perpendicular orientation is called homeotropic anchoring (Fig.8.b), and the tilted orientation is the intermediate of the two configurations. Anchoring can also considered as a surface energy term, which is the last term, , mentioned in 2.1.3. This term so called Rapini-Papoular model, [31], [32]

$$\boldsymbol{f_{rapini}} = -\frac{\boldsymbol{W_0}}{\mathbf{2}} (\mathbf{n} \cdot \mathbf{e_r})^{\mathbf{2}} \quad (7)$$

where W_0 is the anchoring strength constant and e_r is the preferred direction on the boundary surface. In nature, deviations of anchoring from the easy axis in the surface (the maximum value of f_{rapini}) are preferred more energetically than deviations in the perpendicular to the surface (minimum value of f_{rapini}) to minimize total free energy. [9]

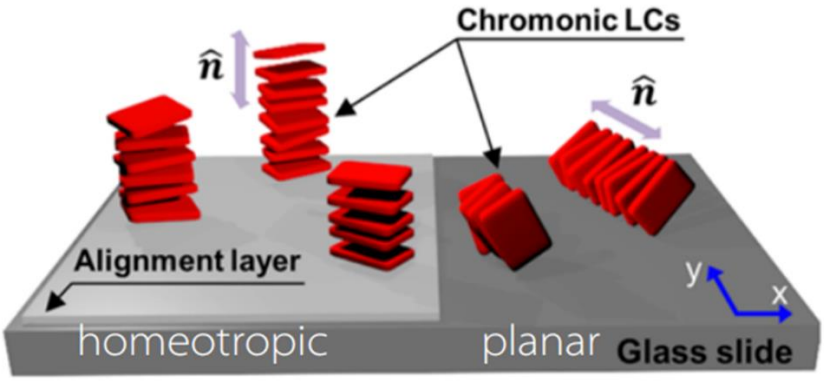

Figure 9 Schematics diagram of the anchoring of SSY on a glass glide and an alignment layer. [33]

Meanwhile, the anchoring of LCLCs differs from the anchoring control technique of TLCs. If it works in same way, the anchoring strength is weak. It is known that homeotropic anchoring of LCLCs is difficult to achieve. In the case of SSY, a methods for homeotropic anchoring in solid interface have been reported which using graphene, parylene films, poly (methyl methacrylate) films, and fluoropolymer films. [33] However, There is no reported case of the homeotropic anchoring of liquid-SSY interface.

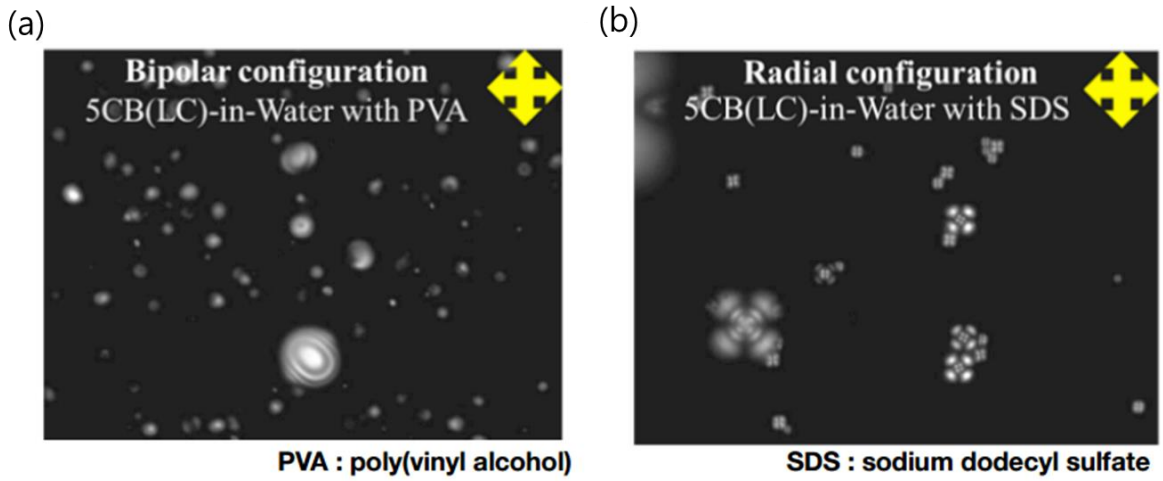

Figure 10 Anchoring control of 5CB droplet. (a) planar LCs droplet using PVA (b) homeotropic LCs droplet using SDS.

The conventional method of controlling the anchoring of LCs and liquid interface was to dilute a surfactant into continuous media. In Fig. 10, PVA and SDS are diluted as surfactant in water, and the planar anchoring condition (Fig. 10.a) and the homeotropic anchoring condition. (Fig.10.b)

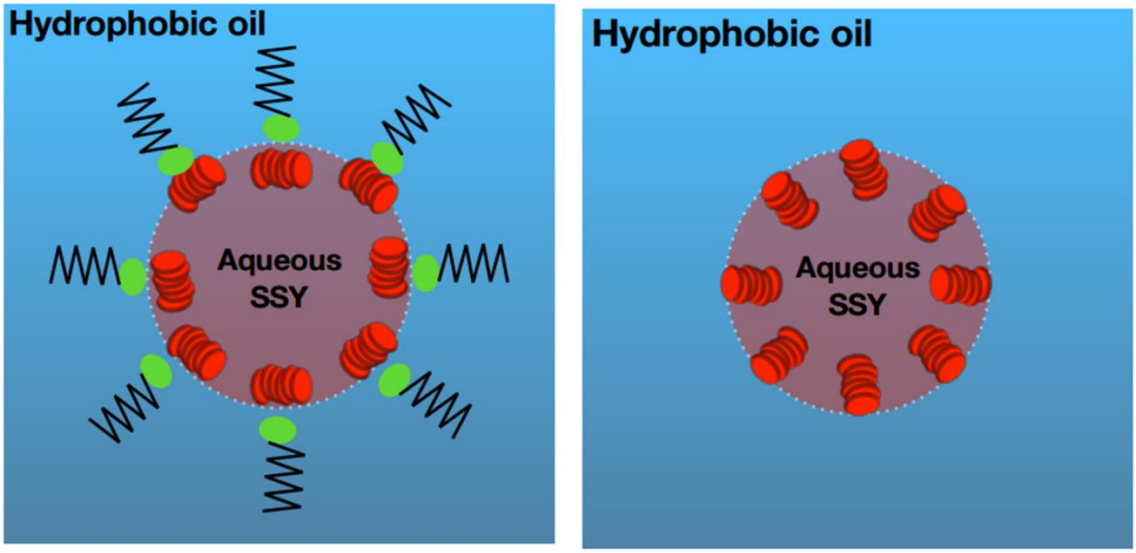

Figure 11 Schematics of SSY droplet with surfactant (a) and without surfactant (b)

On the other hand, in the case of SSY droplet using Surfactant (Fig.11.a), only the planar anchoring configuration appeared regardless of the surfactant .The equilibrium states were that the hydrophilic parts of Surfactant and the hydrophilic part of SSY were facing each other. To find a homeotropic condition, we set a free of surfactant environment. (Fig.11.b). Since the core part of SSY and the hydrophobic oil (Silicone oil) are mutually hydrophobic, they are in contact with each other to form a vertical orientation. But since there was no surfactant, there were issues that the droplets falling to the bottom due to the sedimentation, or the coalescence of the droplets which is the droplets merge together. So, we use a high viscosity silicone to the droplet move as slowly as possible.

III. Experimental setup

3.1 Preparation of LCLCs droplet cells

3.1.1 Sunset Yellow (SSY) purification

SSY uses 90% (wt / wt) dye purchased from Sigma-Aldrich. It is purified using the precipitation method used in other published papers. [6], [34], [35] First, dissolve SSY in deionized water (18.2 MΩ · cm), dissolve ethanol 99.6% (wt / wt) for precipitation, and centrifuge it. Discard the solvent and repeat the above procedure twice. Then, dissolve deionized water and SSY and leave in oven or vacuum oven for one day.

3.1.2 Aqueous Sunset Yellow (SSY) solutions

Purified SSY is dissolved in deionized water at a proper concentration. In this work, the SSY solution was mainly used at a concentration of 30% (wt / wt). To prevent the concentration change due to evaporation of water, it was sealed with Parafilm, and the microtube was dissolved in oven and vortexer.

3.1.3 Brucine sulfate solutions

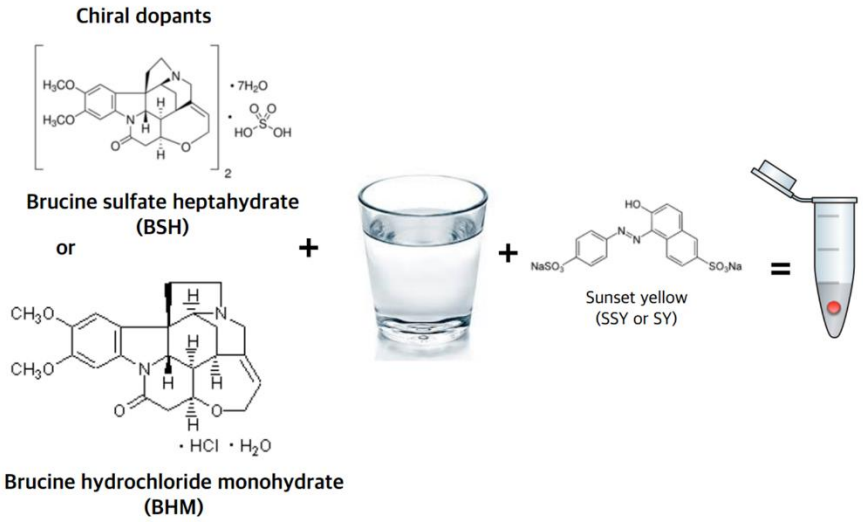

Figure 12 Preparation of SSY doped brucine solution.

Brucine was used as Chiral dopant. In this work, the brucine surfate heptahydrate (BSH) and brucine hydrochloride monohydrate (BHM) were used. First dilute Brucine with water. Brucine aqueous solution was heated and stirred with magnetic bar. because it was hard to dilute with water. and Next, add SSY into the brucine solution. If necessary, deionized water was additionally diluted to dilute the proper concentrations of Brucine and SSY.

3.1.4 Assembly of SSY cells

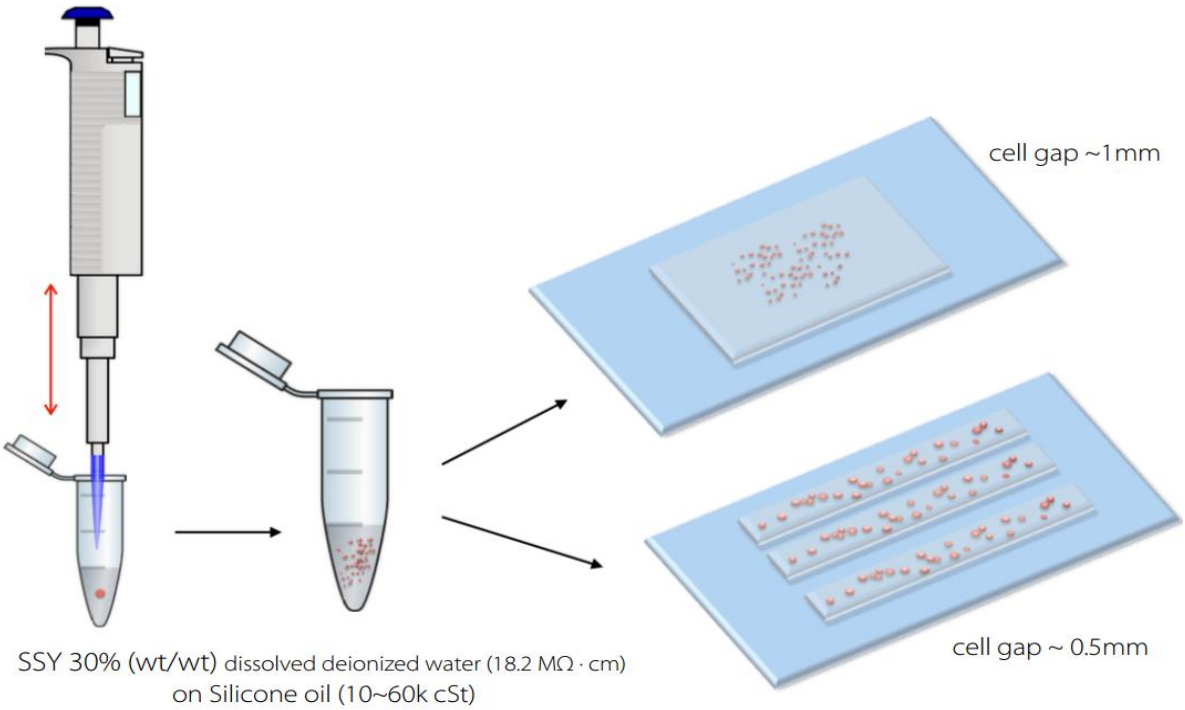

Figure 13. Assembly of SSY droplet cells

To make a droplet sample, inject the aqueous nematic SSY solution (or SSY doped with brucine solution) using a pipette into the silicone oil. Then mix with a pipette tip to make it droplet. We did not use surfactant and we used high viscosity silicone oil (> 30k cSt) to prevent the sedimentation or coalescence of droplets. In the experiment, various manufacturers of silicone oil were used, Shinetsu, Sigma-Aldrich and Gelest's Silicone oil. Then, the cell gap made by using the slide glass is placed in a sandwich cell of about 1 mm or the cell gap is transferred to the capillary of about 5 mm by using the negative pressure.

3.2 Polarized optical microscopy

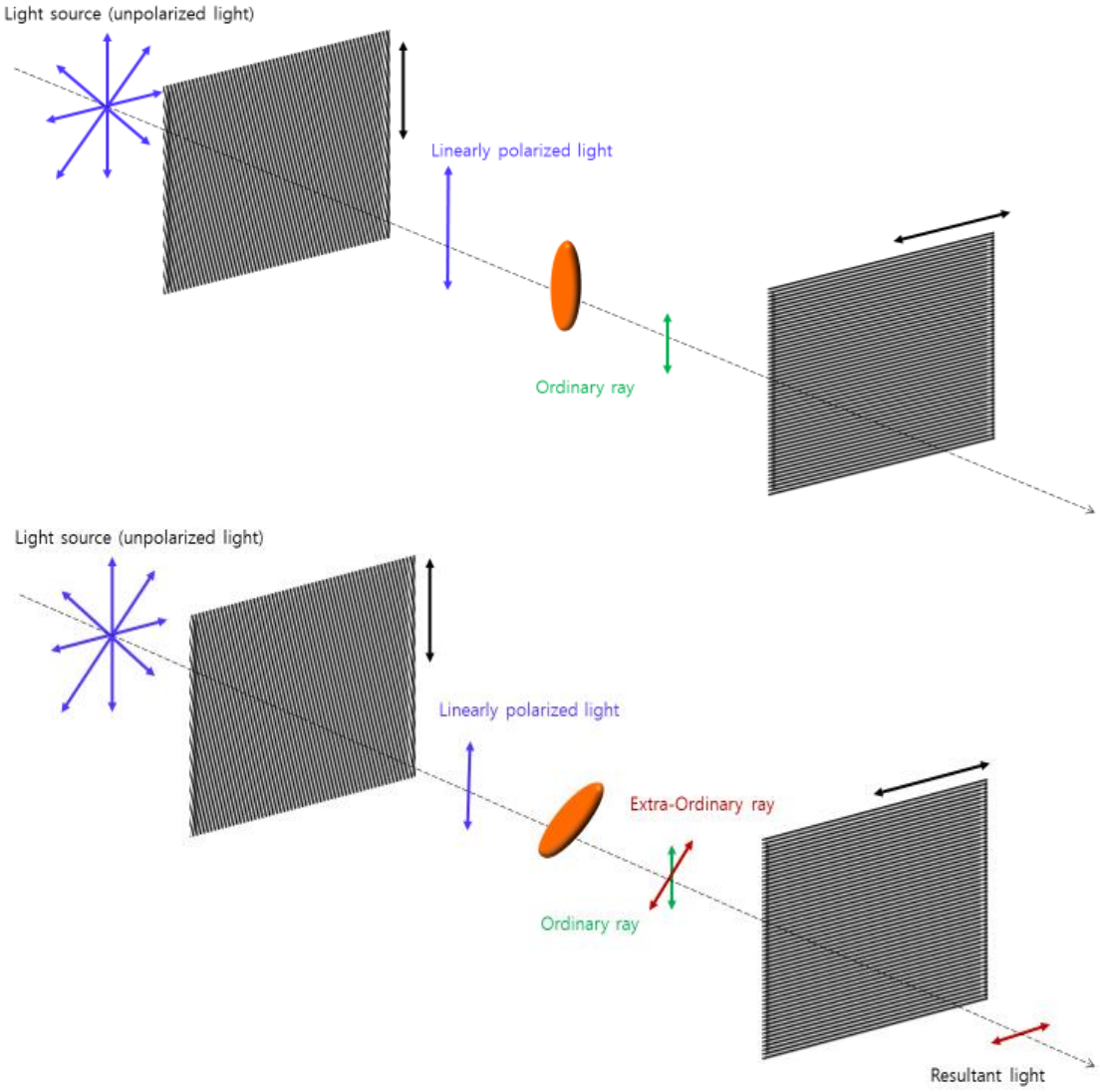

Figure 14. Schematics of the polarized microscopy

Basically, nematic LCs have birefringence properties. To observe and analyze the director structure of LCs, a polarizing microscope is effective tool. This technique is based on the interaction of polarized light and LCs to observe contrast with the background. As refer to Fig13, the fundamental principle of the two microscopes is the same. When light from an unpolarized light source passes through LCs between two polarizers, the intensity observed depends on the state of polarization and the configuration of LCs due to the angle between the polarizers. Also, fundamentally isotropic media is useful for distinguishing between isotropic and anisotropic portions because it cannot transmit light across two polarizers at 90 degrees (crossed polarized condition).We used an upright and inverted

polarizing microscope as shown in Fig 14, The upright and inverted polarizing microscope are the Olympus BX53, IX73 microscopes used in the experiment. The underlying mechanism is the same as in Schematics(Fig13). We used the i-Solution IMT-CCD2 mainly for IX73 inverted microscope for long time measurement (~ 3.83fps) and the BX53 upright microscope for phase transition of LCLCs using a Lumenera Infinity3-6UR (Sony ICX694 CCD sensor) as a heating / cooling stage.

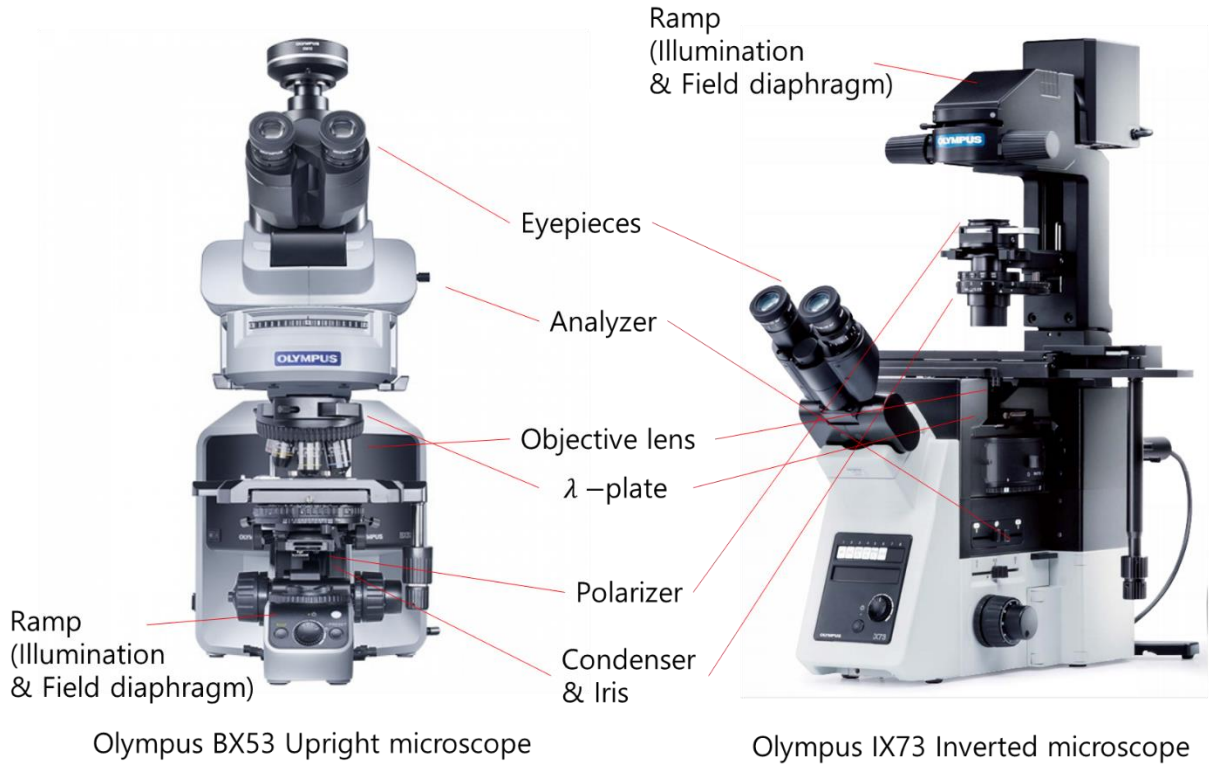

Figure 15. (Left) Upright , (Right) Inverted polarized microscope [36], [37]

IV. Result and Discussion

4.1 Configuration of homeotropic SSY droplets

4.1.1 Radial structure

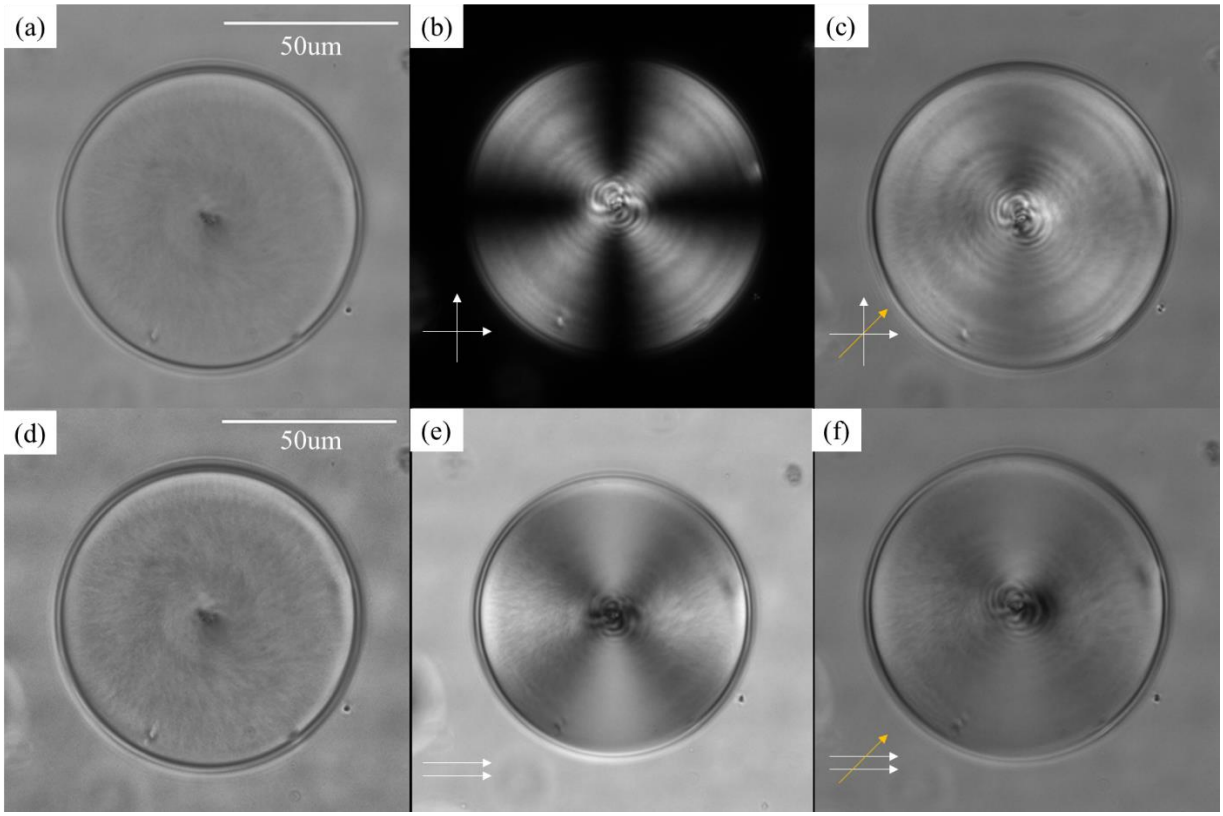

Figure 16 Radial structure of SSY droplet. (a) bright field image (b) cross polarizer image (c) cross pol image with wave plate (d) enhanced scattering on bright field (e) parallel polarizer image (f) parallel polarizer image with wave plate. the white arrow indicates polarization direction (b)-(c) and (e)-(f).

The simplest director structure that can be considered in the sphere droplet with the homeotropic anchoring is a radial structure with a point defect in the droplet structure. This is consistent with the case reported in TLCs. [11], [38], [39] In Fig. 15, we can see that the director structure of the droplet is a radial structure through the cross pol image and the point defect of the polarizing microscope.

4.1.2 Axial structure

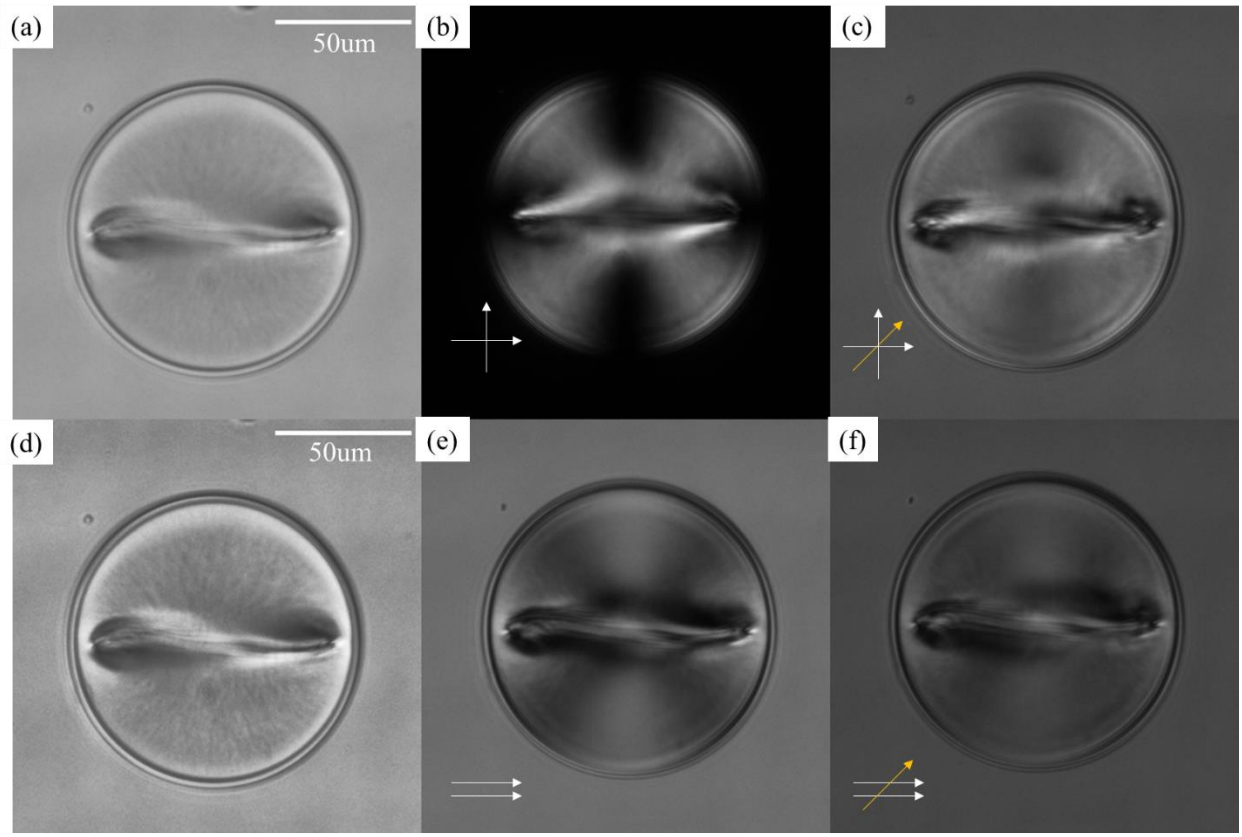

Figure 17 Axial structure of SSY droplet. (a) bright field image (b) cross polarizer image (c) cross pol image with wave plate (d) enhanced scattering on bright field (e) parallel polarizer image (f) parallel polarizer image with wave plate. the white arrow indicates polarization direction (b)-(c) and (e)-(f).

the Interesting thing is that ring disclinations with so-called axial structures have been observed. (Fig 16) These structures do not come out of nature, they are a director structure that can be used when applied an external field or when there is a weak anchoring condition. [40], [41]

As shown Fig 17, Considering the stabilization of each structure as an elastic modulus, the radial structure is inferred to have a relatively small structure of K_1 dominated by splay deformation. Conversely, the axial structure is considered to be a dominant structure of bending with a relatively small K_3. [16] On the other hand, when approaching an anchoring strength, the director structure without anchoring will be stabilized by a side-by-side structure with no deformation at all. (F = 0). However, as the intensity of homeotropic anchoring increases, the homeotropic anchoring boundary propagates to the bulk. it can be stabilized in the axial structure to the radial structure. [40]

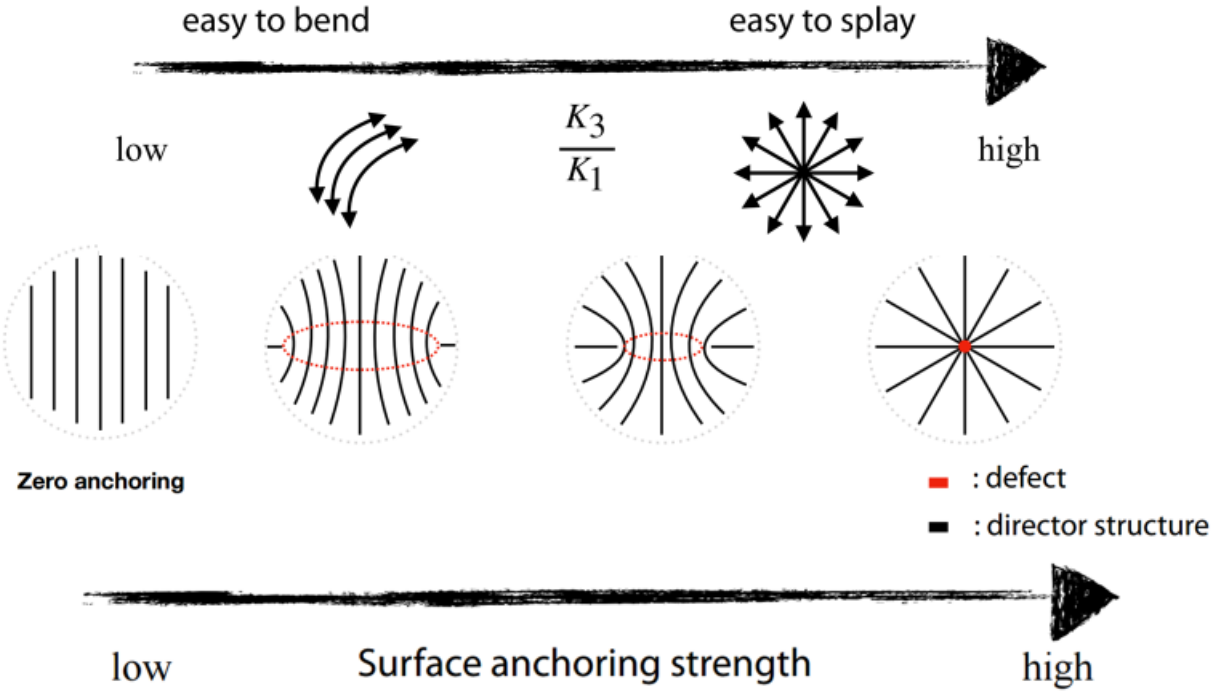

Figure 18 Stable regime of Axial and Radial structures. (Top) The stabilization of the radial and axial structures is determined by the ratio of splay and bend elastic modulus. (Bottom) But also the anchoring strength propagating from the surface to bulk. It explains those structures.

$$F_{24} = -\frac{K_{24}}{2} \int dV \left[\nabla \cdot (\mathbf{n} \times \nabla \times \mathbf{n} + \mathbf{n}\nabla \cdot \mathbf{n})\right]$$
$$= -\frac{K_{24}}{2} \int \boldsymbol{dS} \cdot (\mathbf{n} \times \boldsymbol{\nabla} \times \mathbf{n} + \mathbf{n}\boldsymbol{\nabla} \cdot \mathbf{n}) \quad (8)$$

However, there was an underline issue. If we rewrite the K_{24} term (Eq.8), the saddle-splay term, in the Frank elastic free energy, we can only rewrite it as a term for the surface through the divergence theorem. Since the K_{24} term is a negative term, it is treated as an effective surface anchoring that supports anchoring on the surface. Previous research has shown that only radial structures are stabilized regardless of anchoring strength when $K_{24} > 2K$ ($K_1 \cong K_3$). [40] In case of SSY, the value of K_{24} is about 6 times or more than that of other K_1 or K_3. [42] Nonetheless, the droplets of axial structures still were dominant. The difference between the existing prediction and the theoretical study should be complemented by establishing another model.

4.1.3 Twisted director configuration

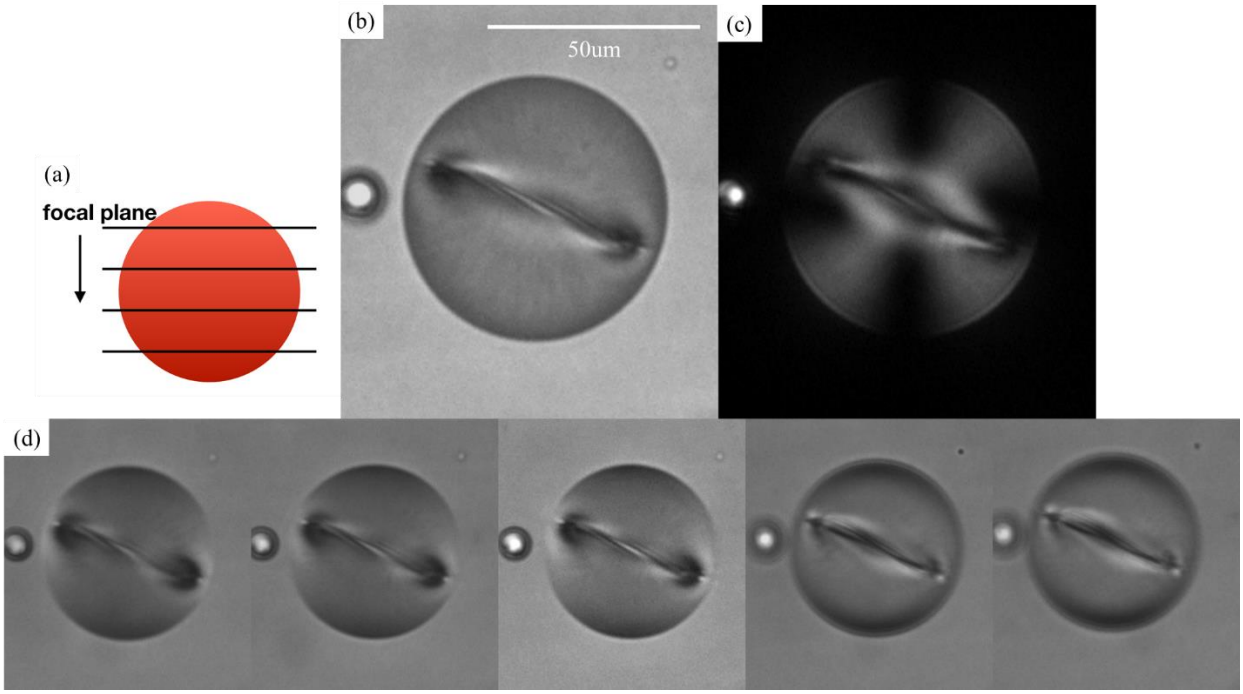

Figure 19 Twist structure of ring disclination. (a) Schematics of changing focal plane image. (b) bright field (c) cross pol (d) changing focal plane image. The ring disclination in the droplet appears to be twisted rather than flat plane ring.

The director structure of the SSY drops, surprisingly, prefers a twisted structure. The planar orientation droplet environment and the structures of the LCLCs confined the capillary favor a twisted structure. [42], [43] The elastic modulus of the LCLCs in Table 2 gives the reason for this. The twist modulus K_2 of LCLCs is significantly lower than the other constants. In other words, the arrangement of LCLCs can be easily modified for twist deformations over other elastic deformation. Fig.18 shows the ring disclination on the focal plane in the axial structure of LCLCs vertical orientation droplets.. Ring disclination is consistent with previous reports, in that the ring does not flat but appears as a twisted ring.

K (pN) @ 25°C	Splay K_1	Twist K_2	Bend K_3	Saddle-splay K_{24}
5CB	6.6	3.0	10	10
Sunset yellow	7.7	1.0	9.5	55

Table 2 Elastic constant of 5CB & SSY [24], [25], [42]

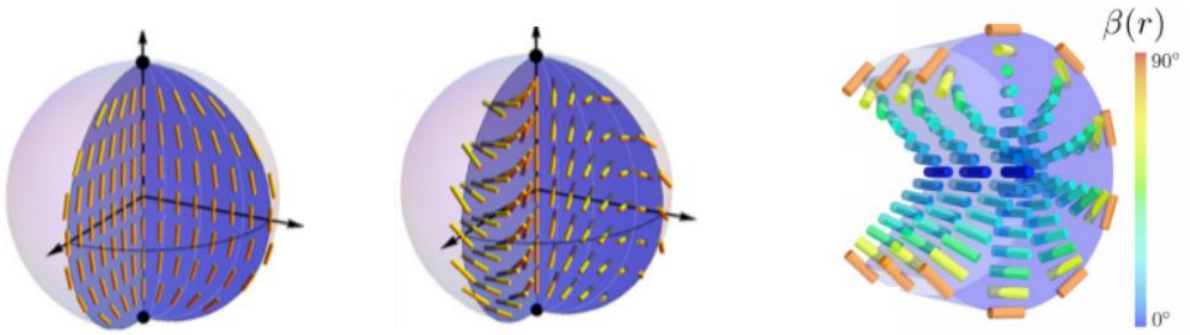

Figure 20 Bipolar structure and Twisted bipolar of LCLCs droplet , LCLCs in capillary.

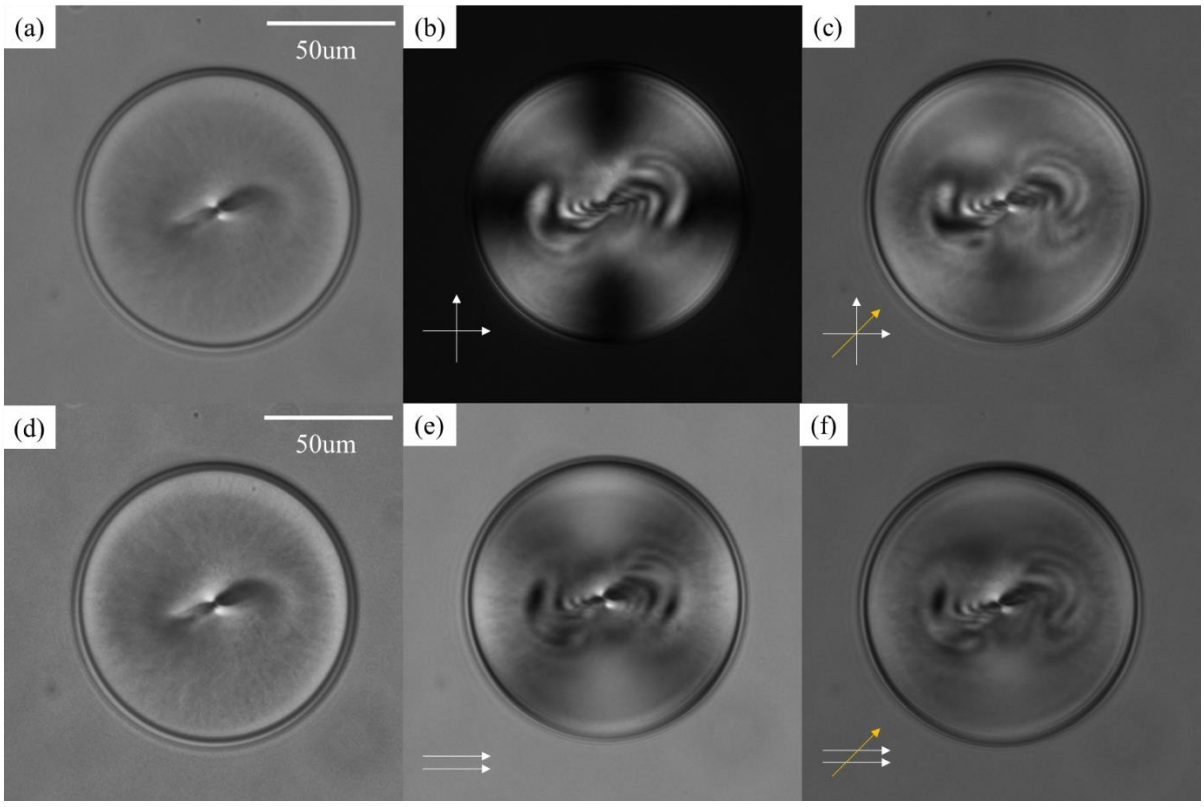

Figure 21 Twisted radial structure. (a) bright field image (b) cross polarizer image (c) cross pol image with wave plate (d) enhanced scattering on bright field (e) parallel polarizer image (f) parallel polarizer image with wave plate. the white arrow indicates polarization direction (b)-(c) and (e)-(f).

Also, the radial structure is inferred as a twisted director structure. Referring to Fig.20, The structure of director is shown as twisted around defect and enhanced image.

4.2 Spontaneous anchoring transition

4.2.1 Axial to bipolar transition

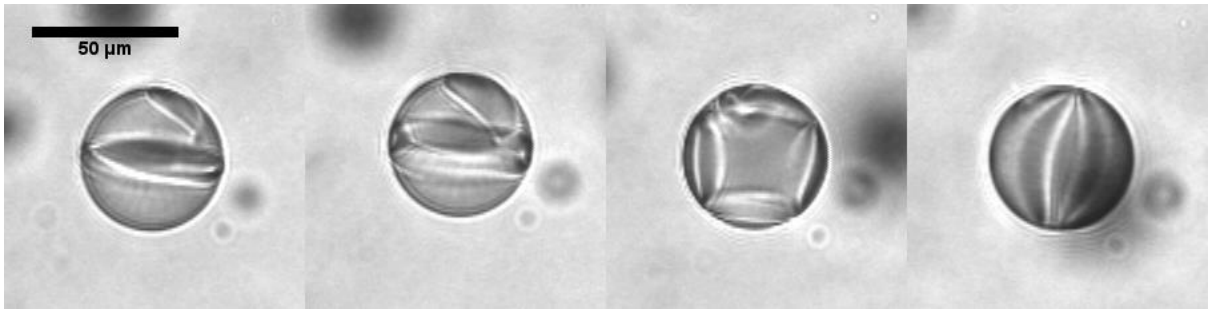

Figure 22 Axial structure to Bipolar droplet transition. each interval of images is 20min. The ring disclination split to double ring. The surface anchoring between double ring is planar. As time goes on, the double ring grow apart to polar point. Finally, the structure of droplet became bipolar droplet.

Another evidence supporting the Weak anchoring mentioned in Section 4.1.2 is that an anchoring transition occurs spontaneously. Because of the very weak anchoring at the interface, the director anchoring at the interface transits to planar anchoring rather than maintaining homeotropic anchoring. As shown in Fig. 21, the ring disclination of the droplet is split, and the spacing between separated rings becomes planar anchoring. As the two rings gradually reach the drop pole, the droplet eventually transitions to a bipolar drop. This process takes about 1 hour.

4.2.2 Speckle texture

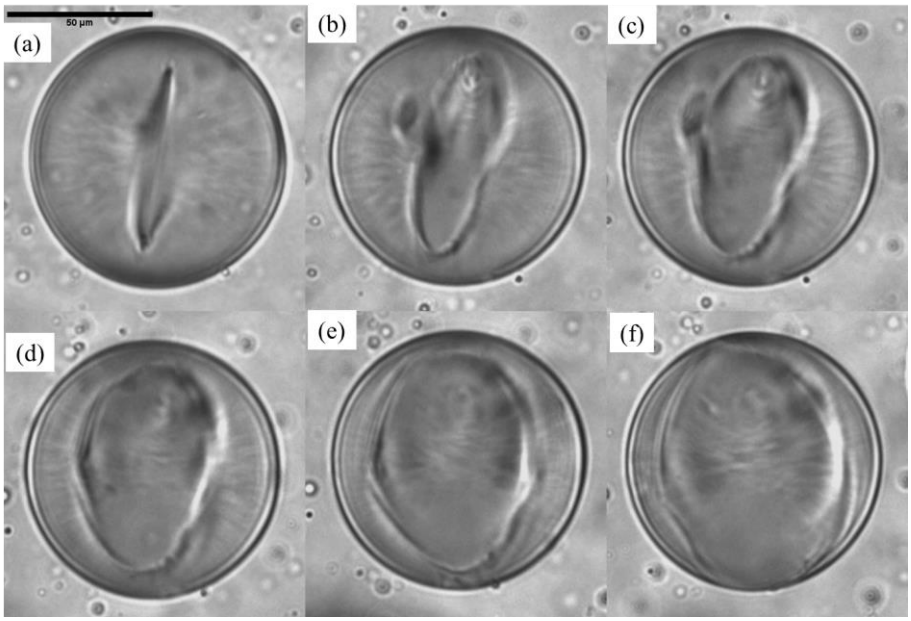

Figure 23 Speckle texture of axial structure droplet. each interval of images is 20min. (a) 0min, (b) 20min, (c) 40min, (d) 60min, (e) 80min (f) 100min. The local domain of the droplet is transferred to planar anchoring, which is also affected by ring disclination.

The anchoring transition occurs in another case which appears as a speckle, as shown in Fig.22 In the case of bipolar transition, the anchoring transits from the edge of the ring, but this is an anchoring transition that occurs in arbitrary localized region. This anchoring transition is broadened over time, as in the previous case, and can be combined with the defect to transform its structure.
Also, as shown in Fig.23, which shows the reorientation of the director by quenching the radial structure droplet with the speckle texture, the droplet that has been heated to the isotropic phase and then cooled to the nematic after the phase transition has speckle texture again. It should be noted that the speckle texture was generated randomly, not in its original position, though it was rearranged into a radial structure. This speckle texture shows that weak anchoring strength that maintains homeotropic is low as in the previous results, and the transition to another anchoring occurs.

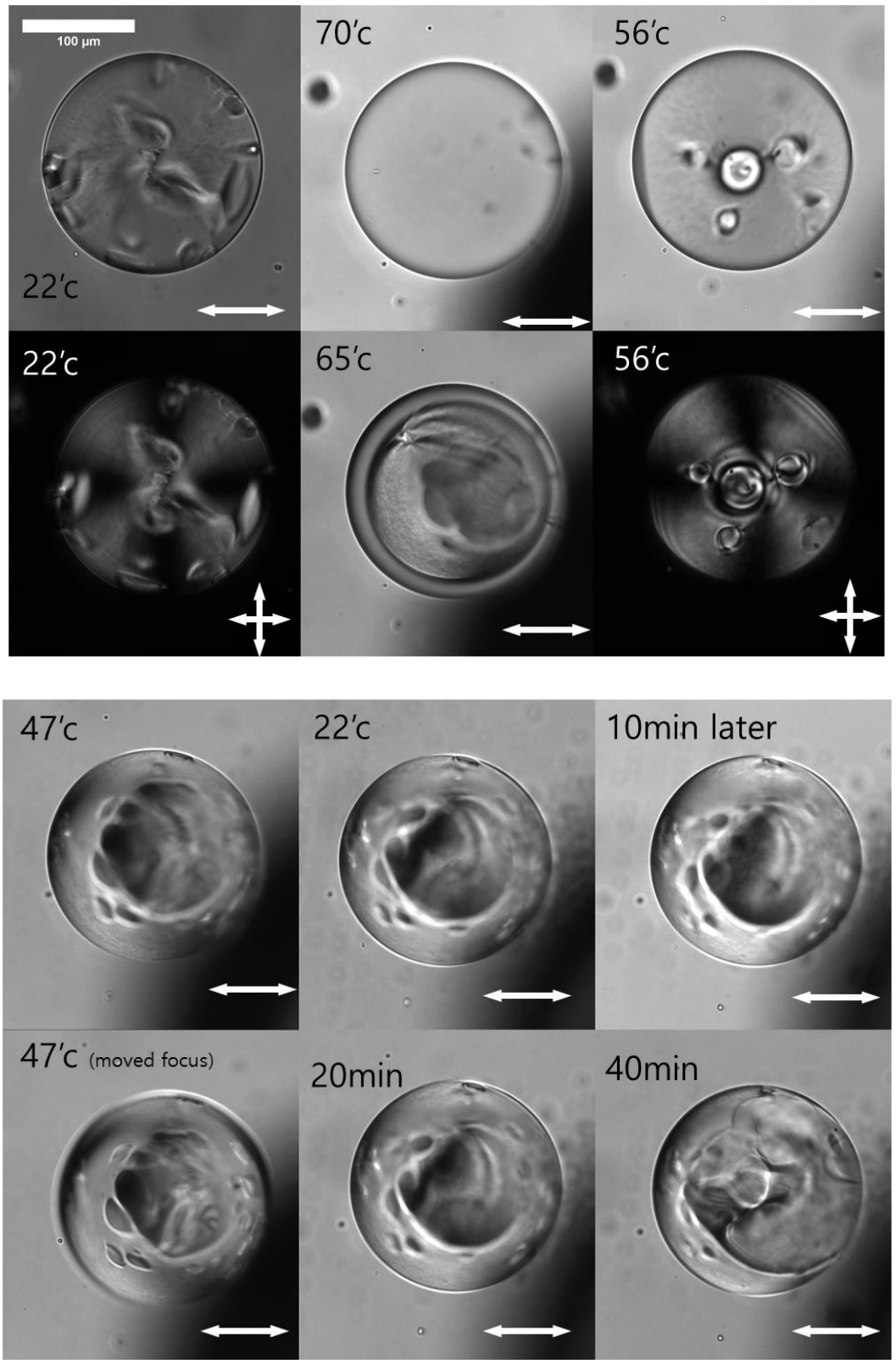

Figure 24 Reorientation radial structure droplet with speckle texture using heating and cooling

4.2.3 Silicone oil dependency

Oil type	Capillary cell	Sandwich cell
Shinetsu Silicone oil 10k cSt	Hard to measure	~ 10 min
Shinetsu Silicone oil 30k cSt	~ 2 hour	~ 2 hour
Gelest Silicone oil 30k cSt	~ 2 hour	~ 2 hour
Shinetsu Silicone oil 50k cSt	~ 4 hour	~ 2 hour
Gelest Silicone oil 60k cSt	~ 3 hour	~ 2 hour
Sigma-Aldrich Silicone oil 60k cSt	~ 6 hour	~ 10 min

Table 3 Silicone oil dependency for the time to form speckle textures

To determine that if the anchoring strength has the dependency of Silicone oil, we made SSY droplet sample using various types of silicone oils. The time written in the table is the time when the speckle texture starts to appear. The 10k cSt Si oil could not be measured in the capillary for a long time due to sedimentation. Relatively slow anchoring transition was observed in the capillary cell compared to the sandwich cell. the time of the Speckle texture varied to manufacturer, but was essentially independent of the viscosity of the Si oil.

4.3 Unexpected structure

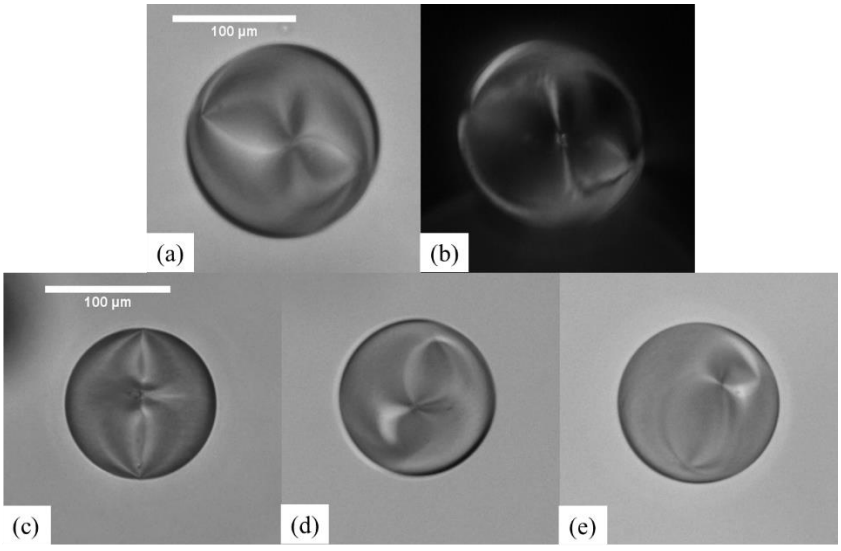

Figure 25 Unexpected structures. (a) bright field, (b) cross pol image of (a), (c)-(e) bright field image

The droplet was injected through a direct injection through a capillary syringe with an inner diameter of about 100 μm. But the unexpected director structure (Fig.24), which had not been reported

previously, appeared. The director structure of this droplet is considered to have three topological defects and has no previously reported structure.

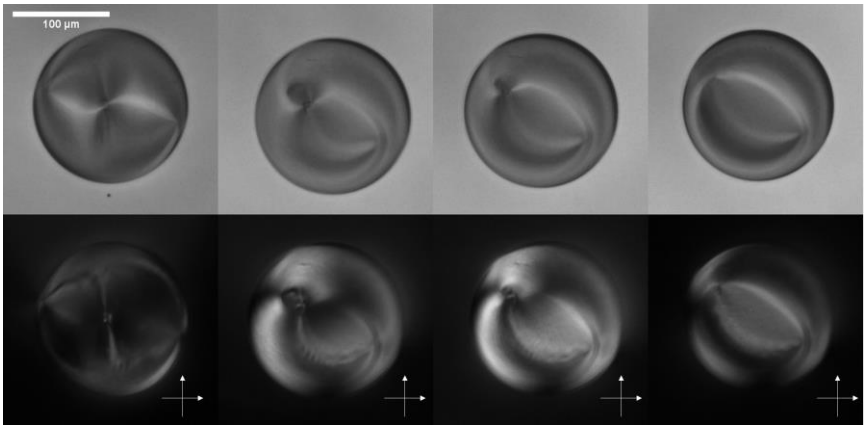

Figure 26 Time evolution of unexpected structure (Top row) bright field (Bottom row) cross pol image. Each image is same droplet. Time interval of each column set is about 20min.

Similar to the results in 4.2, spontaneous anchoring transitions were also observed. (Fig.25) We observed anchoring changes in about 1 hour, and in the initial state, the defects, which were three, merged with each other and turned into bubbles with two defects and observed bipolar structures.

V. Chiral nematic LCLCs

5.1 Pitch measurements

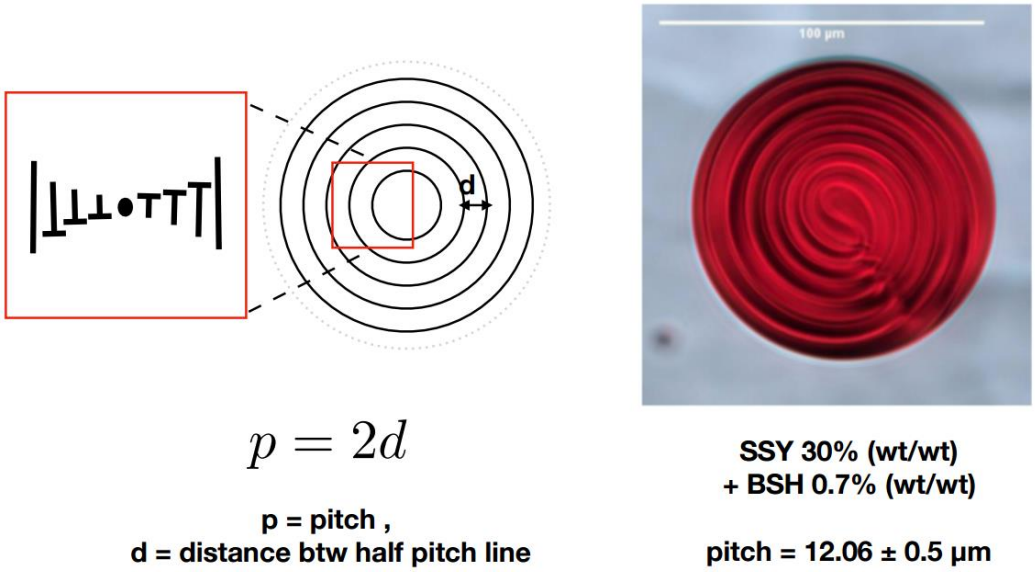

Figure 27 Chiral nematic SSY droplet with planar boundary condition.

We fabricated a chiral nematic SSY planar droplet using the previously reported planar alignment method. [43] Fig. 27 (left), the chiral nematic planar droplet was a structure with a concentric half-pitch line. The distance between half pitch lines was measured to determine the helical twisting power (HTP) values of brucine sulfate heptahydrate (BSH) and brucine hydrochloride monohydrate (BHM). The HTP measured to $\beta_{BSH} = 0.1228 \pm 0.007\ \mu m^{-1}$, $\beta_{BHM} = 0.1102 \pm 0.02\ \mu m^{-1}$.

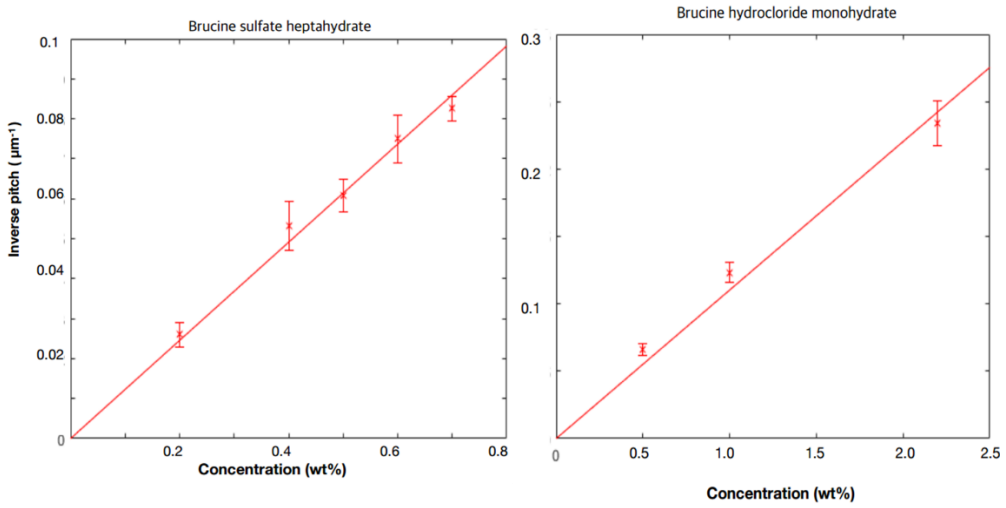

Figure 28 Inverse pitch vs dopants concentration, the concentration of SSY fixed in 30% (wt/wt). the gradient of fitting line is helical twisting power.

5.2 Structures of homeotropic chiral nematic SSY droplets

5.2.1 Definition of N

$$\mathbf{N_0} = \frac{2d}{p_0} \quad (9)$$

To analyze a chiral nematic droplet, define N. N_0 is represented by the droplet diameter d and the chiral pitch p_0. The physical meaning of N is a dimensionless parameter of how many times the director structure makes a half-turn (π turn) through the distance of the droplet diameter. [44] As shown in Fig.26, If N = 2, the director experiences a diameter of the droplet and turns twice a half turn.

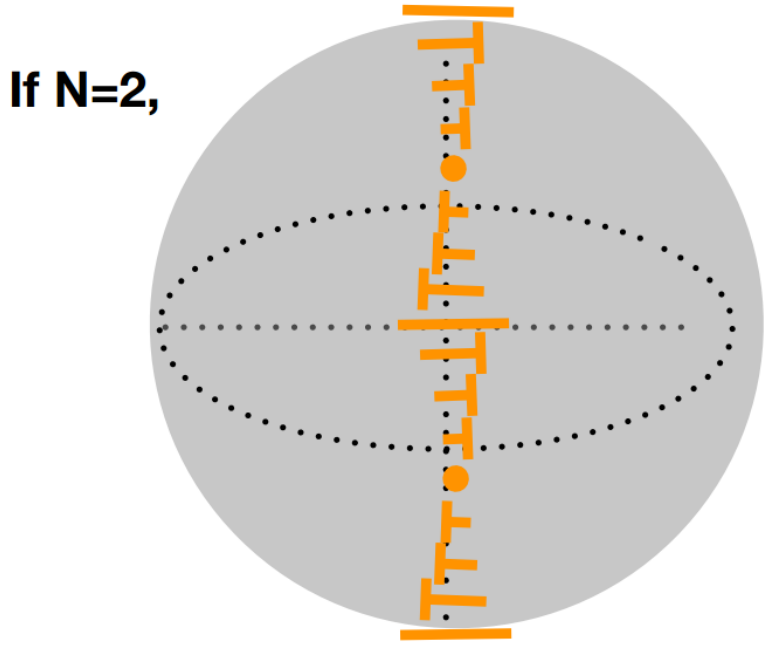

Figure 29 Examination N=2 case of chiral nematic droplet. a director is represented by a nail shape and when the director is 0 degrees, there is no head, and when the director is rotated 90 degrees, it is represented by a point. In the figure above, the director rotates 2 π turn.

5.2.2 Untwisting of helical structure

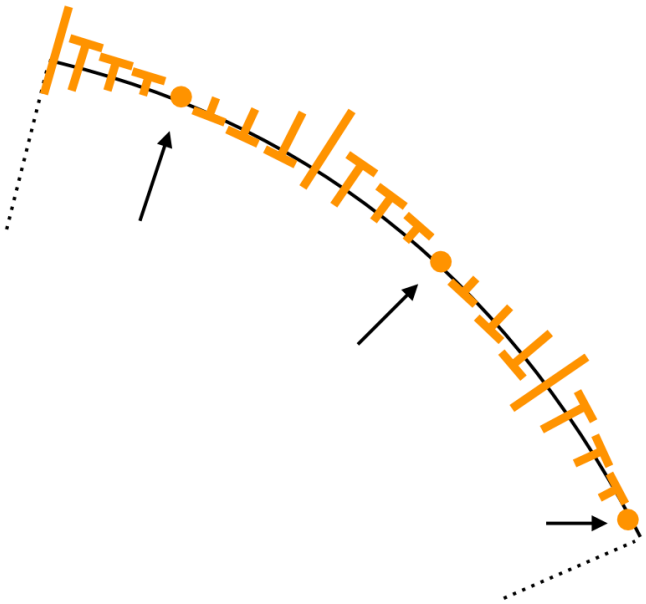

Figure 30 Schematics of homeotropic surface of chiral nematic droplet

Due to the nature of the chiral nematic LCs, the conditions of the homeotropic boundary cannot be established in droplet geometry. Therefore, the homeotropic chiral nematic droplet is observed to be N, which is smaller than the original N_0 in the experiment. It means the pitch look larger in homeotropic droplet. This was reported as untwisting of helical structure. [45]

$$\mathbf{N} = \frac{\mathbf{2d}}{\boldsymbol{p_0}} - \frac{\boldsymbol{b}}{\boldsymbol{d}} = \mathbf{N_0} - \frac{\boldsymbol{b}}{\boldsymbol{d}} \quad (10)$$

N is represented by droplet diameter d, pitch p0, and untwisting coefficient b.

Intrinsic pitch of the helix p_0 at various concentrations C of the chiral addition and the coefficients a and b

C, %	p_0, μm	$2/p_0$, μm^{-1}	a, μm^{-1}	b, μm
3.0	5.5 ± 0.3	0.36 ± 0.02	0.36 ± 0.04	46.7 ± 12.9
4.5	3.7 ± 0.2	0.54 ± 0.03	0.56 ± 0.02	26.9 ± 5.2
6.7	2.4 ± 0.1	0.83 ± 0.04	0.81 ± 0.02	18.3 ± 3.9
7.7	2.0 ± 0.1	1.00 ± 0.05	1.01 ± 0.01	7.9 ± 1.7

Table 4 Chiral dopant concentration dependency using thermotropic chiral nematic LC based on E7(Merck) nematic doped in cholesteryl acetate. (the intrinsic twisting power is 6.1 μm^{-1}.) [45]

The untwisting coefficient b is also related to chirality. It was reported that as the concentration of chiral dopant increases (i.e. as the chirality increases) the b decreases as the pitch increases.

5.2.3 Homeotropic chiral nematic SSY droplet

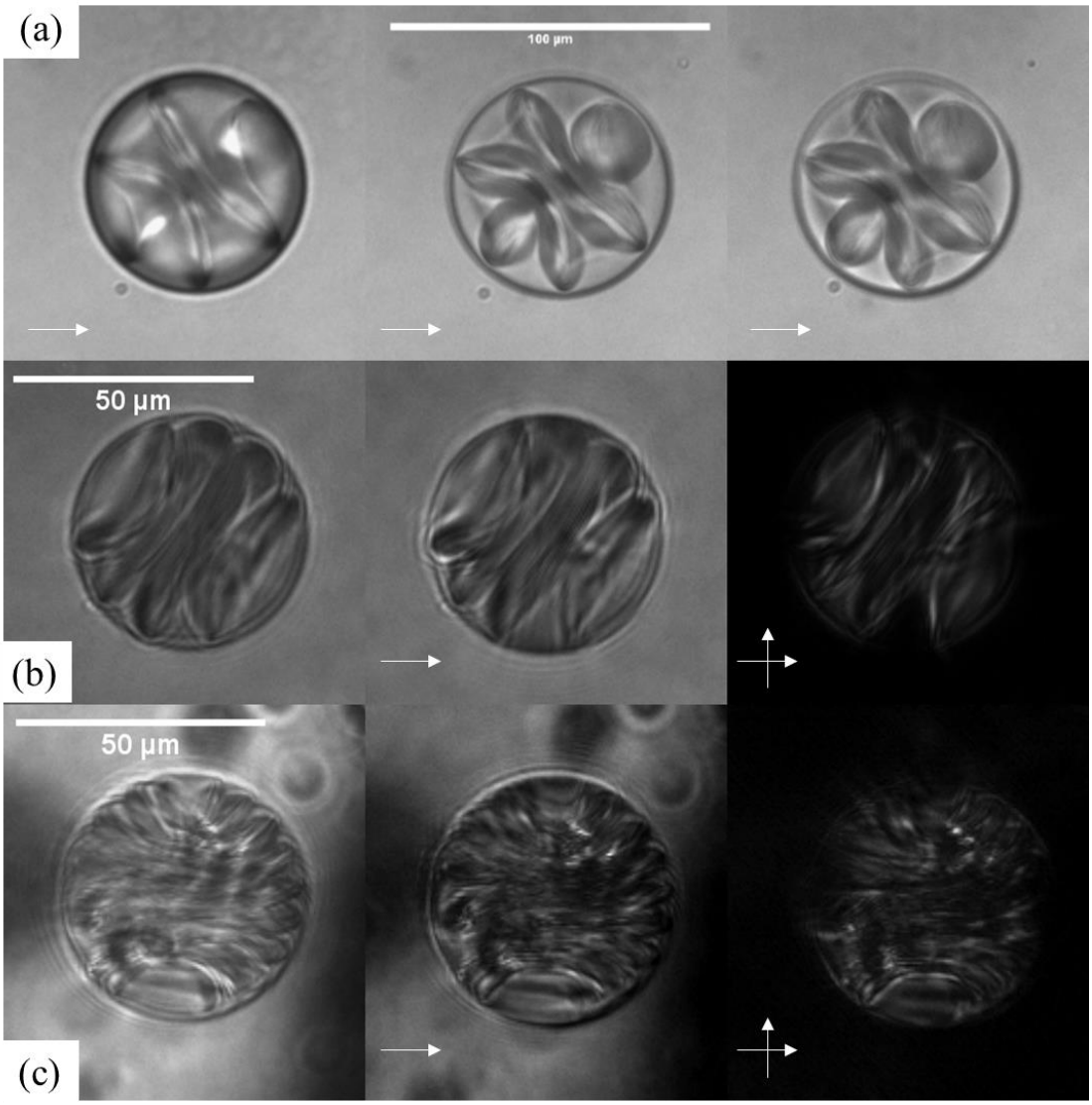

Figure 31 Homeotropic chiral nematic droplet. each row set is same droplet. (a) changing focal plane image. (b)-(c) bright field, polarized image, cross pol image.

Fig. 28 is a chiral nematic SSY drop observed in the experiment. In contrast to the previously reported achiral SSY, the director structure of the droplet is a bipolar configuration with a helical loop defect. [46] Analyzing with N of droplet is consistent with the trend of existing reports. It can be seen that as the concentration of the chiral dopants increases, the pitch decreases and accordingly the untwisting factor b also decreases. LCLCs also show untwisting of helical structures like thermotropic LCs. That is, when the homeotropic droplet is observed, the pitch is longer than the planar droplet of the same concentration. However, this is different from the conventional thermotropic case. Coefficient b was about 10 times as large as that of the thermotropic LCs. The equation modified the Frank free energy density for chiral nematic LCs (Eq.11), where q_0 represents the wave vector in the planar layer of the chiral LCs. In the planar condition, the first term of the equation becomes $q0$ to minimize the free

energy for the elastic deformation, but not in the homeotropic condition. Due to the effect of untwisting, the pitch of the homeotropic droplet becomes larger, so that the first term is smaller than q_0.

$$\mathbf{f_2} = \frac{K_2}{2}\left[\left(\mathbf{n}\cdot\boldsymbol{\nabla}\times\mathbf{n}+\frac{2\pi}{p_0}\right)\right]^2 = \frac{K_2}{2}\left[(\mathbf{n}\cdot\boldsymbol{\nabla}\times\mathbf{n}+\mathbf{q_0})\right]^2 \quad (11)$$

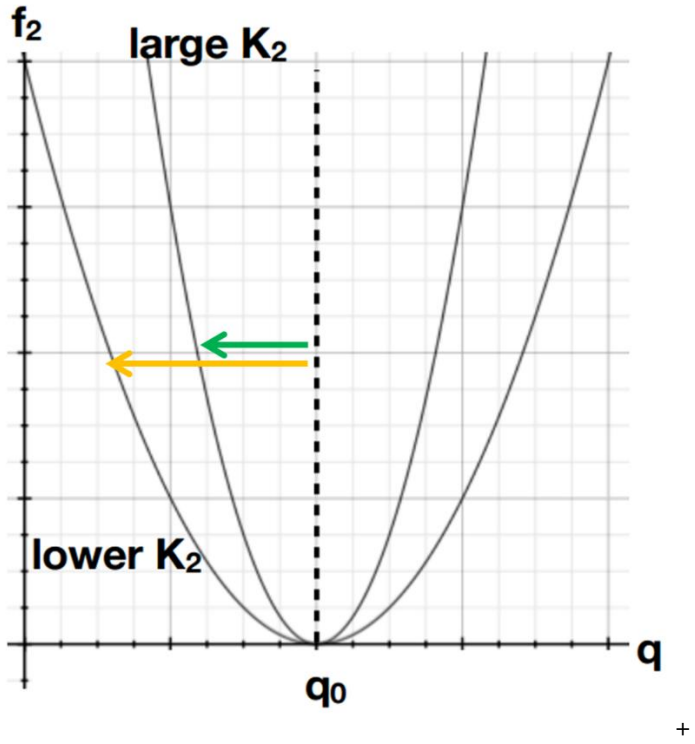

Figure 32 Examination of f_2 respect of q. For LCLCs, the deviation of q_0 is large because of having a small K2.

Even if we have the same energy in Fig. 29, the possible |q| is larger because K2 of LCLCs is very small. Thus, SSY with a very small K2 can have a smaller q value compared to conventional thermotropic LCs. A small q value means that SSY has a larger pitch when untwisting occurs at the homeotropic droplet. (again, q is inverse pitch) This is the reason why the untwisting coefficient b of Chiral nematic SSY is large is explained.

VI. Conclusion

Nematic LCLCs droplet

We have implemented a homeotropic alignment layer between liquid (hydrophobic oil) and SSY interface that has never been reported. We use silicone oil without surfactant to adjust homeotropic anchoring of SSY. In the past reports, radial structures with point defects in thermotropic liquid crystal droplets were mainly observed / reported. However, in the experiment, SSY homeotropic droplet dominated axial structure with ring disclination.
In addition, spontaneous anchoring transition occurred in these axial structures. Homeotropic anchoring droplets were transitioned to planar anchoring and became completely bipolar droplets. From this point of view, our anchoring environment is assumed to be weak anchoring strength. Furthermore, consistent with previous reports, homeotropic SSY droplets favored a twisted director structure. Because of the low K_2 characteristic of LCLCs, the structure of the director is more likely to have twist deformation than other deformation, and consistent with previous reports (twisted bipolar droplet, doubly twisted structure on capillary cell).

Chiral nematic LCLCs

Original SSY has an achiral molecular structure. However, using brucine as a chiral dopant, SSY in the geometry with added chirality was observed as droplet. Brucine sulfate heptahydrate and brucine hydrochloride monohydrate were used and the helical twisting power was determined by measuring the pitch for each concentration. In case of homeotropic chiral nematic SSY droplets, droplets were observed in the non - surfactant silicone oil as in the homeotropic anchoring environment. Due to the homeotropic orientation observed in the chiral nematic thermotropic liquid crystal, a chiral SSY has also been observed in which the pitch is lengthened (i.e. untwisting of helical structure). The untwisting coefficient b of SSY has a considerably large value compared to other liquid crystals, which is inferred to be due to the small K_2 value of the LCLCs in the modified elastic free energy in the chiral nematic liquid crystal.

VII. Reference

[1] M. Schadt and W. Helfrich, "VOLTAGE-DEPENDENT OPTICAL ACTIVITY OF A TWISTED NEMATIC LIQUID CRYSTAL," *Appl. Phys. Lett.*, vol. 18, no. 4, pp. 127–128, 1971.

[2] P. Yeh and C. Gu, *Optics of liquid crystal displays*, 2nd ed., U. Hoboken, N.J. : Wiley, 2010.

[3] M. Humar and I. Muševič, "3D microlasers from self-assembled cholesteric liquid-crystal microdroplets," *Opt. Express*, vol. 18, no. 26, pp. 26995–27003, 2010.

[4] S. Sivakumar, K. L. Wark, J. K. Gupta, N. L. Abbott, and F. Caruso, "Liquid Crystal Emulsions as the Basis of Biological Sensors for the Optical Detection of Bacteria and Viruses," *Adv. Funct. Mater.*, vol. 19, no. 14, pp. 2260–2265, 2009.

[5] I.-H. Lin, D. S. Miller, P. J. Bertics, C. J. Murphy, J. J. de Pablo, and N. L. Abbott, "Endotoxin-induced structural transformations in liquid crystalline droplets.," *Science*, vol. 332, no. 6035, pp. 1297–1300, Jun. 2011.

[6] H. S. Park *et al.*, "Self-assembly of Lyotropic chromonic liquid crystal sunset yellow and effects of ionic additives," *J. Phys. Chem. B*, vol. 112, no. 51, pp. 16307–16319, 2008.

[7] "File:Sort_sol_pdfnet @ en.wikipedia.org." .

[8] "File:School_jacks_klein @ commons.wikimedia.org." .

[9] S. Theses, *Topological Formations in Chiral Nematic Droplets*. .

[10] T. J. Scheffer and J. Nehring, "A new, highly multiplexable liquid crystal display," *Appl. Phys. Lett.*, vol. 45, no. 10, pp. 1021–1023, 1984.

[11] G. E. Volovik and O. D. Lavrentovich, "Topological dynamics of defects: boojums in nematic drops," *Sov. Phys. JETP*, vol. 58, no. December 1983, pp. 1159–1166, 1983.

[12] T. C. Lubensky, D. Pettey, N. Currier, and H. Stark, "Topological defects and interactions in nematic emulsions," *Phys. Rev. E*, vol. 57, no. 1, pp. 610–625, 1998.

[13] M. E. Helgeson, L. Porcar, C. Lopez-Barron, and N. J. Wagner, "Direct observation of flow-concentration coupling in a shear-banding fluid," *Phys. Rev. Lett.*, vol. 105, no. 8, pp. 1–4, 2010.

[14] P.-G. de Gennes, *The physics of liquid crystals*, 2nd ed.. Oxford: Clarendon Press, 1993.

[15] M. Kleman and O. D. Lavrentovich, *Soft Matter Physics: An Introduction*. New York, NY: Springer New York, 2003.

[16] P. S. Drzaic, "Nematic Configurations Within Droplets," *Liq. Cryst. Dispersions*, pp. 99–181, 1995.

[17] M. Ballauff, "Thermotropic liquid crystals, fundamentals. by G. Vertogen und V. A. de Jeu . springer-verlag, Berlin 1988. xi, 324 pp., hard cover, DM 134.00.—ISBN 3-540-17946-1," *Adv. Mater.*, vol. 1, no. 3, p. 93, 1989.

[18] L. Longa, D. Monselesan, and H.-R. Trebin, “An extension of the Landau-Ginzburg-de Gennes theory for liquid crystals,” *Liq. Cryst.*, vol. 2, no. 6, pp. 769–796, 1987.

[19] “Chirality_and_Stereoisomers @ chem.libretexts.org.” .

[20] “Radical_(chemistry) @ en.wikipedia.org.” .

[21] D. Demus and L. Richter, *Textures of liquid crystals*. Deutscher Verlag für Grundstoffindustrie, 1980.

[22] “2008-05-samsung-worlds-blue-phase-technology @ phys.org.” .

[23] L. Joshi, S.-W. Kang, D. M. Agra-Kooijman, and S. Kumar, “Concentration, temperature, and <math display="inline"> <mrow> <mi>p</mi> <mtext>H</mtext> </mrow> </math> dependence of sunset-yellow aggregates in aqueous solutions: An x-ray investigation,” *Phys. Rev. E*, vol. 80, no. 4, p. 041703, Oct. 2009.

[24] R. D. Polak, G. P. Crawford, B. C. Kostival, J. W. Doane, and S. Umer, “Optical determination of the saddle-splay elastic constant K24 in nematic liquid crystals,” *Phys. Rev. E*, vol. 49, no. 2, 1994.

[25] S. Zhou *et al.*, “Elasticity of lyotropic chromonic liquid crystals probed by director reorientation in a magnetic field,” *Phys. Rev. Lett.*, vol. 109, no. 3, 2012.

[26] S. Zhou *et al.*, “Elasticity, viscosity, and orientational fluctuations of a lyotropic chromonic nematic liquid crystal disodium cromoglycate.,” *Soft Matter*, vol. 10, no. 34, pp. 6571–81, 2014.

[27] K. Nayani *et al.*, “Spontaneous emergence of chirality in achiral lyotropic chromonic liquid crystals confined to cylinders,” *Nat. Commun.*, vol. 6, p. 8067, Aug. 2015.

[28] S. Zhou, *Lyotropic Chromonic Liquid Crystals*. 2017.

[29] P. J. Collings, A. J. Dickinson, and E. C. Smith, “Molecular aggregation and chromonic liquid crystals,” *Liq. Cryst.*, vol. 37, no. 6–7, pp. 701–710, 2010.

[30] N. H. Hartshorne and G. D. Woodard, “Mesomorphism in the System Disodium Chromoglycate-Water,” *Mol. Cryst. Liq. Cryst.*, vol. 23, no. 3–4, pp. 343–368, 1973.

[31] A. RAPINI and M. PAPOULAR, “Distorsion D’Une Lamelle Nématique Sous Champ Magnétique Conditions D’Ancrage Aux Parois,” *Le J. Phys. Colloq.*, vol. 30, no. C4, pp. C4-54-C4-56, 1969.

[32] M. Nobili and G. Durand, “Disorientation-induced disordering at a nematic-liquid-crystal--solid interface,” *Phys. Rev. A*, vol. 46, no. 10, pp. R6174--R6177, 1992.

[33] J. Jeong, G. Han, A. T. C. Johnson, P. J. Collings, T. C. Lubensky, and A. G. Yodh, “Homeotropic alignment of lyotropic chromonic liquid crystals using noncovalent interactions,” *Langmuir*, vol. 30, no. 10, pp. 2914–2920, 2014.

[34] V. R. Horowitz, L. A. Janowitz, A. L. Modic, P. A. Heiney, and P. J. Collings, “Aggregation

behavior and chromonic liquid crystal properties of an anionic monoazo dye," *Phys. Rev. E - Stat. Nonlinear, Soft Matter Phys.*, vol. 72, no. 4, pp. 1–10, 2005.

[35] D. J. Edwards, J. W. Jones, O. Lozman, A. P. Ormerod, M. Sintyureva, and G. J. T. Tiddy, "Chromonic liquid crystal formation by edicol sunset yellow," *J. Phys. Chem. B*, vol. 112, no. 46, pp. 14628–14636, 2008.

[36] "a71e1dd63d3f456825efe6ff229b725f33066ef8 @ www.olympus-lifescience.com." .

[37] "ebe76a81d90b5be2339ab3b7b4dcb37e6526d057 @ www.olympus-lifescience.com." .

[38] O. O. Prishchepa, V. Y. Zyryanov, a. P. Gardymova, and V. F. Shabanov, "Optical Textures and Orientational Structures of Nematic and Cholesteric Droplets with Heterogeneous Boundary Conditions," *Mol. Cryst. Liq. Cryst.*, vol. 489, no. 1, p. 84/[410]-93/[419], 2008.

[39] O. Prishchepa, a. Shabanov, and V. Zyryanov, "Director configurations in nematic droplets with inhomogeneous boundary conditions," *Phys. Rev. E*, vol. 72, no. 3, p. 031712, 2005.

[40] S. Žumer and S. Kralj, "Influence of k24 on the structure of nematic liquid crystal droplets," *Liq. Cryst.*, vol. 12, no. 4, pp. 613–624, 1992.

[41] A. Sonnet, A. Kilian, and S. Hess, "Alignment tensor versus director: Description of defects in nematic liquid crystals," *Phys. Rev. E*, vol. 52, no. 1, pp. 718–722, 1995.

[42] Z. S. Davidson *et al.*, "Chiral structures and defects of lyotropic chromonic liquid crystals induced by saddle-splay elasticity," *Phys. Rev. E*, vol. 91, no. 5, pp. 1–5, 2015.

[43] J. Jeong, Z. S. Davidson, P. J. Collings, T. C. Lubensky, and a G. Yodh, "Chiral symmetry breaking and surface faceting in chromonic liquid crystal droplets with giant elastic anisotropy.," *Proc. Natl. Acad. Sci. U. S. A.*, vol. 111, no. 5, pp. 1742–7, 2014.

[44] T. Orlova, T. Yamaguchi, N. Katsonis, and E. Brasselet, "Creation and manipulation of topological states in chiral nematic microspheres," no. May, 2015.

[45] M. N. Krakhalev, A. P. Gardymova, A. V. Emel'yanenko, J.-H. Liu, and V. Y. Zyryanov, "Untwisting of the helical structure of cholesteric droplets with homeotropic surface anchoring," *JETP Lett.*, vol. 105, no. 1, pp. 51–54, 2017.

[46] M. N. Krakhalev *et al.*, "Bipolar configuration with twisted loop defect in chiral nematic droplets under homeotropic surface anchoring," *Sci. Rep.*, vol. 7, no. 1, pp. 2–11, 2017.